

A Marked Point Process Approach For Identifying Neural Correlates of Tics in Tourette Syndrome

Carlos A. Loza, Jonathan B. Shute, Jose C. Principe, Michael S. Okun, and Aysegul Gunduz

Abstract—We propose a novel interpretation of local field potentials (LFP) based on a marked point process (MPP) framework that models relevant neuromodulations as shifted weighted versions of prototypical temporal patterns. Particularly, the MPP samples are categorized according to the well known oscillatory rhythms of the brain in an effort to elucidate spectrally specific behavioral correlates. The result is a transient model for LFP. We exploit data-driven techniques to fully estimate the model parameters with the added feature of exceptional temporal resolution of the resulting events. We utilize the learned features in the alpha and beta bands to assess correlations to tic events in patients with Tourette Syndrome (TS). The final results show stronger coupling between LFP recorded from the centromedian-parafascicular complex of the thalamus and the tic marks, in comparison to electrocorticogram (ECoG) recordings from the hand area of the primary motor cortex (M1) in terms of the area under the curve (AUC) of the receiver operating characteristic (ROC) curve.

Index Terms—Marked Point Process, LFP, Tourette Syndrome, Transient Model

I. INTRODUCTION

Local field potentials characterize the mesoscopic electrical activity in the brain. In particular, they reflect the synchronized average spatiotemporal interactions brought about by graded excitatory postsynaptic potentials (EPSP's) and inhibitory postsynaptic potentials (IPSP's) [1]. When compared to electroencephalogram (EEG), the inherent invasive nature of LFP provides finer spatial resolution and improved SNR levels. This allows for specific targeting of cortical and subcortical structures for uncovering the relationship between internal physiological processes and/or external stimuli.

Tourette Syndrome is a childhood-onset neuropsychiatric disorder that comprises motor and phonic tics that may be accompanied by other neuropsychiatric comorbidities [2], [3]. Its pathophysiology remains unknown; hypotheses include hyperactive dopaminergic neurons in the cortico-striato-thalamo-cortical circuit, abnormally increased cortical excitability, and dysfunction of basal ganglia dopaminergic structures [4]. In terms of therapies, deep brain stimulation (DBS) constitutes a suitable alternative when pharmacological methods are no longer an option [5].

Carlos A. Loza and Jose C. Principe are with the Computational NeuroEngineering Laboratory (CNEL), University of Florida, Gainesville, FL (email: cloza@ufl.edu, principe@cnel.ufl.edu).

Michael S. Okun is with the Department of Neurology, Division of Movement Disorders, University of Florida, Gainesville, FL (email: okun@neurology.ufl.edu).

Jonathan B. Shute and Aysegul Gunduz are with the J. Crayton Pruitt Family Department of Biomedical Engineering, University of Florida, Gainesville, FL (email: jbshute@bme.ufl.edu, agunduz@bme.ufl.edu).

This work was supported by NSF CAREER 1553482 and NIH R01NS096008 grants.

In particular, adaptive DBS (aDBS) has been proved efficient in Parkinson's Disease by monitoring the ongoing LFP in an effort to provide proper feedback and prompt stimulation [6]. Hence, a similar approach can be applied to TS patients. We focus on DBS recordings from the centromedian-parafascicular complex of the thalamus (CM-PF) and ECoG from the hand primary motor cortex (M1) during tic events scored by a clinician. We exploit a novel framework for neuronal oscillations that poses relevant events as the result of marked point process samples activating finite impulse response filters over time. In this way, the temporal resolution is preserved up to the sampling frequency scale and the resulting features can be further utilized to understand the underlying mechanisms operating during tics in TS patients.

The rest of the paper is organized as follows: Section 2 introduces the transient model for neuronal oscillations. Section 3 describes the methods utilized to estimate the model parameters while Section 4 details the experimental setting. Section 5 presents the main results, and, lastly, Section 6 concludes the paper and discusses further research.

II. TRANSIENT MODEL FOR LFP

One of the hallmarks of neuronal oscillations (EEG, ECoG or LFP) is their transient nature, i.e. weak, short-living local perturbations can affect large parts of the network and exhibit long-lasting effects. Moreover, the ever-changing functional and synaptic connectivity in the brain provides the necessary temporal windows for short-lived oscillations that appear, disappear and reoccur depending on external stimuli processing and/or internal states of the network [7]. We propose a novel generative, multiple input-single output (MISO) framework that is based on a multivariate shot noise model [8]. In particular, it models neuronal oscillations (or EEG for short) as the output of the convolution between weighted Kronecker delta trains and finite temporal filters. The proposed model is illustrated in Fig. 1 or in equations:

$$x[n] = n_0[n] + \hat{x}[n] = n_0[n] + \sum_{i=1}^L y_i[n] \quad (1)$$

$$y_i[n] = \sum_{j=1}^{n_i} \sum_{m=-\infty}^{\infty} \alpha_{i,j} \delta[n - \tau_{i,j} - m] d_{i,\omega_j}[m] \quad (2)$$

where $x[n]$ is an EEG-like signal that represents a single-channel trace, $n_0[n]$ is the noise component with $1/f$ spectral distribution [9]. Each $y_i[n]$ consists of the convolutions between weighted, shifted Kronecker deltas and indexed temporal patterns contained in the filter bank or dictionary,

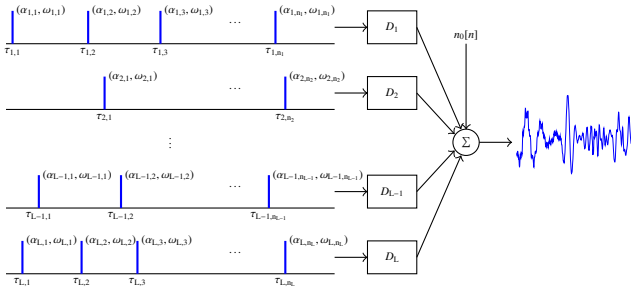


Fig. 1: Transient Model. A single-channel EEG trace is modeled as the noisy addition of reoccurring, transient events over time.

D_i , i.e. $D_i = \{d_{i,\omega_j}\}$. The number of filter banks or atoms, L , is set depending on the frequency bands under analysis; in particular, the behavioral-related distinctions of the oscillatory rhythms make them ideal for this task. The set $\{(\tau_i, \alpha_i, \omega_i)\}_i$ can be conceived as the timestamps and features of a MPP, respectively; in this way, we devise a novel framework for decomposition and analysis of EEG where the temporal resolution has a lower bound set by the sampling rate.

III. METHODS

We begin by focusing on an individual frequency bands; in this way, the decomposition task reduces to multiple single input-single output (SISO) problems. Furthermore, we require a double sparsity constraint regarding the relevant neuromodulations or phasic events; we assume no overlap between adjacent monoscale patterns, and also, a relevant event has to be encoded by only one shifted weighted version of a dictionary atom. This last constraint goes against classical decomposition schemes that only represent EEG segments, e.g. Fourier Transform, and conforms more closely to sparse decomposition techniques that strive to parsimoniously represent EEG traces [10]. With these constraints in mind, we proceed to make use of greedy decomposition methods in an effort to efficiently estimate the MPP samples and filter bank components in an unsupervised fashion.

Our approach mimics the well known clustering technique k-means [11]. Particularly, we choose K M -sample initial dictionary seeds from the set $\{\tilde{y}_i[n]\}_{i=1}^P$ that represents a multidimensional array with P trials from single-channel, bandpassed traces with variable length; this initial dictionary is chosen according to the modulatory patterns present in the sequences, i.e. the envelope is estimated via the Hilbert Transform and patterns with clear maximum close to the midline ($M/2$) are selected. Then, we use the frequency domain (FFT) to efficiently compute the convolutions that encode the temporal sequences and further select the patterns with ℓ_2 -norm above a certain threshold γ . The resulting extracted snippets are normalized and stacked in a matrix $Y \in \mathbb{R}^{M,\Lambda}$ with corresponding assignment indexes $\{\Omega_j\}_{j=1}^\Lambda$. Alg. 1 summarizes the encoding stage.

The outputs from Alg. 1 constitute the inputs for the second stage of the optimization: dictionary update. We utilize the first principal component from the samples corresponding to a particular dictionary atom as the update for such filter.

In a way, it replaces the centroids computation in k-means by the principal component estimation in this M -dimensional space. We refine the optimization by replacing the inherent second-order statistics of singular value decomposition by a robust analysis via the correntropy measure [12]. For two random variables X and Y , correntropy is defined as:

$$V_\sigma(X, Y) = \mathbf{E}[G_\sigma(X - Y)] \quad (3)$$

where $G_\sigma(X - Y)$ is the Gaussian kernel with parameter σ , also known as kernel width. Specifically, we maximize the correntropy of the error between the original input space and the low-dimensional representation. The non-convex nature of the cost function demands for an alternative procedure; for this case, we opted for the half-quadratic (HQ) technique [13] that only requires a stopping threshold for successive estimated bases (set equal to 10^{-4}). One of the main advantages of such optimization is the simultaneous estimation of σ by exploiting Silverman's rule [14]; hence, it does not require additional free parameters. The final dictionary update algorithm is omitted due to space limitations, however, readers interested in the specifics can refer to [15], [16].

Likewise k-means, our decomposition approach is greedy and, consequently, prone to local minima. To avoid such cases and obtain a locally optimal solution, we alternatively iterate between both stages for a fixed number of iterations or when the difference between successive dictionary updates falls below a threshold (10^{-4}). Lastly, we utilize mutual coherence [17] as the selection criterion for multiple dictionaries corresponding to different initial conditions:

$$\mu(D) = \max_{i \neq j} |d_i^T d_j| \quad (4)$$

where d_i is the i -th atom from dictionary D . We select the filter bank with the minimum $\mu(D)$ that provides the less ambiguous decomposition. In summary, we introduce an estimation technique that attempts to extract and cluster relevant phasic events in EEG based only on two main free parameters: the duration (in samples) of putative phasic events, M , and the number of atoms, K .

IV. EXPERIMENTAL SETTING

The first subject is a 23-year-old female with tics that are dystonic in appearance and comprise full arm extensions, shoulder jerks, neck twisting, grimacing, forceful upward eye movements, and occasionally groans. Most of the tics were lateralized to the right side of her body. The second subject is a 25-year-old female; her tics included cursing, yelling, blinking, snorting, finger tapping, and head bobbing. A majority of the tics were centralized to the face. Both subjects provided informed consent as approved by the University of Florida Institutional Review Board (IRB-01) and by the US Food and Drug Administration (FDA) through an investigational device exemption (IDE).

High resolution T1+Gad and FGATIR MRI [18] alongside a deformable brain atlas were utilized for target planing of both bilateral 4-contact CM-PF thalamic DBS leads

Algorithm 1 EEG Decomposition (EEGDecomp).

Inputs: $\{\tilde{y}_i[n]\}_{i=1}^P, M, D, \gamma$
Outputs: $\{(\tau_j, \alpha_j, \omega_j)\}_{j=1}^{n_i}\}_{i=1}^P$
 $j \leftarrow 1$
for $i = 1, \dots, P$ **do**

 CONTINUE = TRUE, $k \leftarrow 1$
 $C = \text{conv2D}(\tilde{y}_i^T[n], \tilde{D})$
 $r_i[n] \leftarrow \max\{|C|, 2\}$
 $\pi_i[n] \leftarrow \arg \max\{|C|, 2\}$
while CONTINUE == TRUE **do**
 $\eta \leftarrow \arg \max_n r_i[n]$
if $|C[\eta][\pi_i[\eta]]| \leq \gamma$ **then**
 $\alpha_k \leftarrow C[\eta][\pi_i[\eta]]$
 $\tau_k \leftarrow \eta - M/2$
 $\omega_k \leftarrow \pi_i[\eta]$
 $Y[:,j] \leftarrow \tilde{y}_i^T[\tau_k - M/2 : \tau_k + M/2] / \alpha_k$
 $\Omega_j \leftarrow \omega_k$
 $k \leftarrow k + 1, \quad j \leftarrow j + 1$
else

 CONTINUE = FALSE, $n_i \leftarrow k$
end if
end while
end for
 $\Lambda \leftarrow j$

(Medtronic 3387, Medtronic, LLC, Minneapolis, MN) and bilateral 4-contact motor cortical subdural strip electrodes (Medtronic Resume II) through one frontal burr hole on each side of the skull. Since many tics involved hand and/or arm movements, the ECoG grid was placed over the hand motor cortex. The DBS microelectrode was positioned and advanced using a micropositioner (FHC, Bowdoin, ME) along the planned thalamic trajectory to allow for physiological monitoring. The resulting traces were further low-passed and downsampled to 800 Hz to capture LFP activity alone.

V. RESULTS

We bandpassed the multi-trial traces from each channel utilizing $Q \approx 1$ Butterworth filters. Then, according to time-frequency analysis and previous studies [19], [20], we deemed the alpha (8–12 Hz) and beta (13–30 Hz) bands as relevant by studying the relative power modulation with respect to the categorized tic marks, i.e. $L = 2$. Then, after thorough visual inspection of the bandpassed traces in the time and frequency domains, we estimated the average duration of the alpha and beta neuromodulations equal to 500 and 400 ms. (350 ms. for Subject 2), respectively. Next, we selected a wide range of dictionary atoms (2^1 – 2^6) to assess its potential effect over behavioral correlates, and, finally, the threshold, γ , was chosen according to a surrogate probability density function (PDF) estimated directly from data.

The surrogate PDF is derived from $\{\beta_M(\tilde{y}[n])_k\}_k$, or simply $\beta_M(\tilde{y}[n])$, which represents the set of ℓ_2 -norms corresponding to the M -sample long snippets from the tensor $\{\tilde{y}_i[n]\}_{i=1}^P$ ($P = 5$ for both subjects). However, this transform is not just a

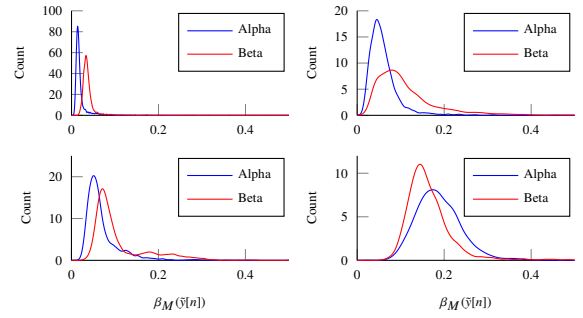


Fig. 2: Estimated PDF of normalized $\beta_M(\tilde{y}[n])$. Row 1: Subject 1. Row 2: Subject 2. Column 1: CM-PF. Column 2: M1.

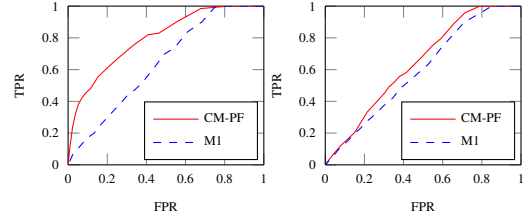


Fig. 3: ROC curves of tic detectors exploiting alpha and beta Marked Point Processes. Left. Subject 1. Right. Subject 2.

mere embedding, it is rather a mapping that emphasizes the modulated patterns present in the bandpassed LFP traces. It starts by extracting the snippets with locally maximum envelope close to the $M/2$ mark and, then, proceeds to extract the remaining unmodulated M -dimensional vectors until no samples are left. In this way, $\beta_M(\tilde{y}[n])$ can be conceived as the power distribution in the filtered recordings with respect to an M -dimensional space that strives to preserve the local temporal structure of the data. Furthermore, we exploit this PDF to sample potential γ values that are fed to Alg. 1.

In short, we estimate $\beta_M(\tilde{y}[n])$ for each band and determine the decomposition threshold based on a range of percentile-based values (0 to 100) from a surrogate PDF. Fig. 2 depicts the estimated $\beta_M(\tilde{y}[n])$ densities for the aforementioned M parameters. They resemble the work done by Freeman when analyzing ECoG during different behavioral tasks [9]; however, he focused on the instantaneous amplitude of the analytic signal alone, while here, we incorporate the temporal structure of the data via the M -dimensional embedding.

After extracting the putative phasic events in both bands and channels according to Alg. 1, we proceeded to match their timestamps to the categorized tic marks. In particular, given the sparse nature of the MPP samples and in order to obtain smooth outputs, we connected temporally adjacent neuromodulation events if their separation was smaller than 500 and 400 ms. (350 ms. for Subject 2), for alpha and beta rhythms, respectively. Next, we considered a hit when one of the two spectral MPPs was active during a scored tic, or a miss otherwise. Thus, we exploit the information from both frequency bands to implement a tic detector. We computed the True Positive Rate (TPR) and False Positive Rate (FPR) in order to characterize the ROC curve of the on-line detector.

TABLE I: AUC of ROC curves for different K 's.

Subject	Sensor	K					
		2	4	8	16	32	64
1	CM-PF	0.80	0.80	0.80	0.81	0.80	0.80
1	M1	0.63	0.64	0.65	0.65	0.64	0.64
2	CM-PF	0.64	0.64	0.64	0.64	0.65	0.65
2	M1	0.60	0.60	0.60	0.61	0.61	0.61

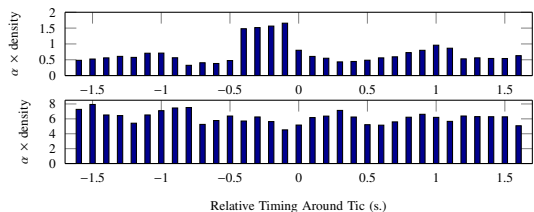


Fig. 4: Distribution of MPP amplitudes times densities over tic trials. Subject 1. Beta band. Top: CM-PF. Bottom: M1. $\gamma = 0$

As Fig. 3 suggests, the CM-PF thalamus electrode provides more discriminant information, while the M1 electrode underperforms in both cases. A useful measure to quantitatively compare scenarios is the area under the curve (AUC) of the ROC plots. Table I shows such measures alongside the final results for every attempted value of K . Clearly, the thalamus sensor for Subject 1 shows stronger predictive power, while, on the other hand, the remaining electrodes remain around the 0.65 mark. A potential reason might have to do with the specific shapes of $\beta_M(\tilde{y}[n])$ depicted on Fig. 2. The estimated PDFs for the best case present well differentiated peaks with small variance; conversely, the remaining densities exhibit more overlapping PDFs with wider peaks. This can be translated as more concentrated activity versus more diffuse non-target specific neuromodulations, respectively. In addition, Table I reveals very consistent measures over K , which suggests a restricted set of prototypical phasic events.

Fig. 4 depicts the histogram of the MPP amplitudes times the phasic event densities or occurrences; this distribution clearly illustrates an average increase of beta activity (CM-PF) starting roughly 500 ms. before tic onset. This can be interpreted as a relatively increased density of higher-amplitude phasic events prior to a tic event. The M1 electrode, however, does not show such discriminative predictive nature and should be subject of further study. Furthermore, Fig. 5 depicts the timestamps of the MPP samples for a particular threshold value. It is evident that the estimated neuromodulations are tightly coupled to the scored tic marks.

VI. CONCLUSIONS

We exploited an MPP interpretation of LFP in order to elucidate behavioral correlates during tics in Tourette Syndrome patients. The results show a relatively clearer discriminative nature from the thalamus region and a less apparent correlation from M1. In the future, we can utilize the particular estimated prototypical atoms, i.e. D , and further investigate the parameter γ to accurately track the changes between tic and non-tic stages in order to provide proper feedback in closed-loop DBS experiments.

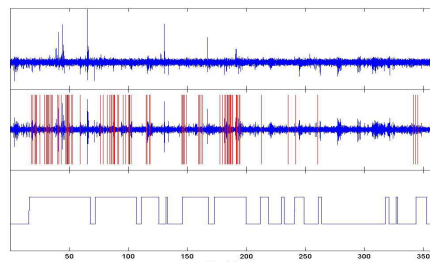


Fig. 5: Top: Raw CM-PF trace. Middle: Bandpassed (beta) CM-PF trace in blue. τ of extracted phasic events in red. Bottom: Tic marks (low level: no tic, high level: tic). Subject 1. $\gamma = 0.04$

REFERENCES

- [1] E. Niedermeyer and F. L. da Silva, *Electroencephalography: Basic principles, clinical applications, and related fields*. Lippincott Williams & Wilkins, 2005.
- [2] J. Jankovic and R. Kurlan, "Tourette syndrome: evolving concepts," *Movement disorders*, vol. 26, no. 6, pp. 1149–1156, 2011.
- [3] A. Gunduz and M. S. Okun, "A review and update on tourette syndrome: where is the field headed?" *Current neurology and neuroscience reports*, vol. 16, no. 4, pp. 1–13, 2016.
- [4] L. Almeida, D. Martinez-Ramirez, P. J. Rossi, Z. Peng, A. Gunduz, and M. S. Okun, "Chasing tics in the human brain: development of open, scheduled and closed loop responsive approaches to deep brain stimulation for tourette syndrome," *Journal of clinical neurology*, vol. 11, no. 2, pp. 122–131, 2015.
- [5] V. Vandewalle, C. van der Linden, H. Groenewegen, and J. Caemaert, "Stereotactic treatment of Gilles de la Tourette syndrome by high frequency stimulation of thalamus," *The Lancet*, vol. 353, no. 9154, p. 724, 1999.
- [6] S. Little, A. Poghosyan, S. Neal, B. Zavala, L. Zrinzo, M. Hariz, T. Foltynie, P. Limousin, K. Ashkan, J. FitzGerald *et al.*, "Adaptive deep brain stimulation in advanced parkinson disease," *Annals of neurology*, vol. 74, no. 3, pp. 449–457, 2013.
- [7] G. Buzsaki, *Rhythms of the Brain*. Oxford University Press, 2006.
- [8] A. Papoulis, "Random variables, and stochastic processes," 1990.
- [9] W. J. Freeman, "Mass action in the nervous system," 1975.
- [10] P. Durka and K. Blinowska, "Analysis of eeg transients by means of matching pursuit," *Annals of biomedical engineering*, vol. 23, no. 5, pp. 608–611, 1995.
- [11] A. Gersho and R. M. Gray, *Vector quantization and signal compression*. Springer Science & Business Media, 2012, vol. 159.
- [12] W. Liu, P. P. Pokharel, and J. C. Principe, "Correntropy: properties and applications in non-gaussian signal processing," *IEEE Transactions on Signal Processing*, vol. 55, no. 11, pp. 5286–5298, 2007.
- [13] R. T. Rockafellar, "Convex analysis (princeton mathematical series)," *Princeton University Press*, vol. 46, p. 49, 1970.
- [14] B. W. Silverman, *Density estimation for statistics and data analysis*. CRC press, 1986, vol. 26.
- [15] R. He, B. Hu, W. Zheng, and X. Kong, "Robust principal component analysis based on maximum correntropy criterion," *IEEE Transactions on Image Processing*, vol. 20, no. 6, pp. 1485–1494, 2011.
- [16] C. A. Loza and J. C. Principe, "Unsupervised robust detection of behavioral correlates in ECoG," in *Neural Engineering, 2017. 8th International IEEE/EMBS Conference on*. IEEE, 2017, p. to appear.
- [17] D. L. Donoho and X. Huo, "Uncertainty principles and ideal atomic decomposition," *IEEE Transactions on Information Theory*, vol. 47, no. 7, pp. 2845–2862, 2001.
- [18] A. Sudhyadhom, I. U. Haq, K. D. Foote, M. S. Okun, and F. J. Bova, "A high resolution and high contrast MRI for differentiation of subcortical structures for DBS targeting: the fast gray matter acquisition T1 inversion recovery (FGATIR)," *NeuroImage*, vol. 47, pp. T44–T52, 2009.
- [19] S. Mallat, *A wavelet tour of signal processing*. Academic press, 1999.
- [20] J. B. Shute, M. S. Okun, E. Opri, R. Molina, P. J. Rossi, D. Martinez-Ramirez, K. D. Foote, and A. Gunduz, "Thalamocortical network activity enables chronic tic detection in humans with tourette syndrome," *NeuroImage: Clinical*, vol. 12, pp. 165–172, 2016.